

Adaptive RGB Color Lexicographical Ordering Framework Using Statistical Parameters From the Color Component Histogram

JOSÉ LUIS VÁZQUEZ NOGUERA¹, CHRISTIAN E. SCHAEERER¹, JACQUES FACON²,
AND HORACIO LEGAL AYALA¹, (Member, IEEE)

¹Facultad Politécnica, Universidad Nacional de Asunción, San Lorenzo 2160, Paraguay

²Department of Computer and Electronics, Universidade Federal do Espírito Santo, São Mateus 29932-540, Brazil

Corresponding author: José Luis Vázquez Noguera (jlvazquez@pol.una.py)

This work was supported by the CONACYT, Paraguay, under Grant 14-POS-007.

ABSTRACT In image filtering, the classical lexicographical ordering is a popular method that cannot be directly applied for ordering colors in RGB color images. This is due to the fact that each color has similar importance and no order can be defined trivially *a priori*. In this work we propose an adaptive color lexicographical ordering framework for RGB color images where a color pixel is transformed into a real number. This transformation is weighted by statistical parameters from each color component histogram and used as the main component for color comparison. This approach seeks to avoid the arbitrariness since the order of the color component priorities is defined by the information extracted from the image itself. The proposed approach was tested by applying a median filter to reduce noise and a morphological approach to local contrast enhancement. In noise reduction, we compare our method with classical ordering techniques on images with different noise levels. Results show that our proposal outperformed the state-of-the art methods according to the Mean Absolute Error (MAE) measure, especially in those scenarios with higher noise levels. In contrast enhancement, the proposed framework outperformed the classical lexicographical ordering method according to Contrast Improvement Ratio (CIR) metric, especially when increasing the contrast factor. Our proposal generates less distortion than the state-of-the art methods ordering.

INDEX TERMS Ordering methods, lexicographical order, statistical parameters, color component histogram.


I. INTRODUCTION

The management of digital images has become an area of interest in different disciplines such as medicine, astronomy, etc. Because of this, image processing has arisen as a topic of interest to get insight from digital images. Color is probably the most important information of all visual elements because it is the fastest stimulus that reaches the brain and affects the central nervous system of people [1].

In image processing, color space is a mathematically structured model so that color and the features associated with it (saturation, lightness, etc.) can be represented by tuples of numbers as, for example, the *RGB*, *CMYK* and *HSI* color spaces. Different color spaces with different properties have been proposed in the literature. Some of the most used color models are $L^*a^*b^*$ [2], *HSL* [3], *CIELAB* [4], *HSI* [5],

HSV [6], and the *RGB* color space [7]–[9]. However, color ordering in most color spaces is a non trivial problem, and it is needed in many well known mathematical procedures of image processing [10].

In particular, color mathematical morphology requires color ordering to define its basic operations, and extend all other operations. Mathematical morphology (MM) is the *de facto* standard mathematical approach to many applications of image processing, such as filtering, noise reduction, contrast enhancement, among others. Based on set theory, lattice theory, topology, and random functions, its analysis and processes geometrical structures [11], [12]. MM was originally developed for binary images and it was later extended to grayscale images. Actually, it is currently being extended to color images. The main challenge for applications of color MM continues to be the selection of an appropriate color space and the ordering [13]–[24].

The associate editor coordinating the review of this manuscript and approving it for publication was Tao Zhou .

In color ordering, lexicographical ordering is one of the most popular methods in the literature [10], [25], because of its desirable theoretical properties and the possibility to customize the way in which image components can be compared [3], [10], [26]–[28]. Louverdis *et al.* [28] and Vardavoulia *et al.* [29] present an *HSV* based lexicographical ordering method for the morphological processing of color images. In [30], Louverdis *et al.* propose a new morphological technique for size and shape analysis of color granular images. Angulo and Serra [31] present a lexicographical ordering method in *RGB* and *HSL* color spaces for *JPEG* color image compression. Ortiz *et al.* [32] used the lexicographical ordering $I \rightarrow H \rightarrow S$ ($H_{ref} = 0^\circ$) for Gaussian noise reduction.

The main weakness for lexicographical ordering is that most decisions are based on the first component, which ignores all other components [4]. To overcome this limitation some lexicographical order variations have been proposed. Angulo [33] and Sartor and Weeks [34] added a distance measurement to a reference color in the first component, to include information of the entire vector. Zamora [11] and Angulo [27] introduced a parameter α to reduce the number possible values of the components. This causes more colors to collide in the component, and increase the likelihood to use all components on the comparisons. Bouchet *et al.* [35] used fuzzy logic to assign the same ordering weight to all of the color components. In [36], Bibiloni *et al.* generalize fuzzy mathematical morphology to process multivariate images in such a way as to overcome the problem of defining an order between colors.

An alternative to lexicographical ordering is to order colors based on the distance function [37]. Distance to a reference color is commonly used for color ordering. Some works propose the automatic reference color selection for MM [38], [39]. Wang *et al.* [40] induce the *RGB* color distance and establish the structural hypergraph in color images. In the $L^*a^*b^*$ space, the Euclidean norm (distance to the origin $L = 0$, $a = 0$ and $b = 0$) is often used as an ordering method for pixels to evaluate the quality of color reproduction, or in color image compression techniques [41]. This strategy keeps a small norm difference between visually similar colors, however different colors may have the same norm. This problem increases when using the *RGB* color space. Following the proposal by Comer and Delp [42], which uses the Euclidean norm and a black pixel as reference in the *RGB* space, two *RGB* colors may appear to be partially equal to the eye but very different based on their norm values. Therefore, the use of these strategies are not recommended in general color ordering.

In [43], Deborah *et al.* propose several basic ordering relations for spectral data. Two ordering relations are extended from the classical marginal and lexicographical ordering, followed by several other ordering relations that are constructed using the total amount of energy and distance function. Sinha *et al.* [44] define a ordering of three-dimensional *RGB* color space using Hilbert 3D space filling curve and

then applies MM operators to obtain the contrast enhanced image.

In *RGB* color images, the bit mixing ordering has proven to be efficient for color image filtering [45], although it prioritizes the red component. Ideally, the most important component will be determined by local information in the image.

In this work we propose an adaptive color ordering framework for the *RGB* color images that is based on local statistical parameters from each color component histogram. A statistical parameter is a number that is obtained from the data of a statistical distribution. Statistical parameters are used to synthesize the information given by a graph.

The colors are ranked according to a weight obtained from the statistical parameters. Further contributions derived from the framework can be summarized as follows:

- We propose the use of several statistical parameters extracted from the local histogram by color component to establish a color ordering. In particular, mode, mean, minimum, maximum, variance and smoothness are used.
- We propose two strategies to extract local characteristics of an image. The first is based on neighborhoods around each pixel, and the second is based on non-overlapping partitions of the image.
- We establish a robust evaluation for noise reduction. This evaluation analyzes the performance of the methods when increasing the noise for different noise types.
- Analogously, we extend a simple contrast enhancement proposal by Stojic *et al.* [46], to analyze the enhancement on the image for different contrast values. The extension adds an enhancement factor, which increases the amount of contrast in the image.

The rest of this article is organized as follows. Section 2 presents the framework. Section 3 explains the applications tested together with some examples of them. Section 4 shows the experimental results of the framework in comparison to the methods suggested in the literature in noise reduction and contrast enhancement using mathematical morphology applications. The conclusions and future Work are presented in Section 5.

II. $\hat{\mathcal{R}}$ ORDERING IN *RGB* COLOR IMAGES

Let an image be a function $f : \mathbb{Z}^2 \rightarrow \mathbb{Z}^3$, where each pair $(x, y) \in \mathbb{Z}^2$ denotes a pixel and $f(x, y) \in \mathbb{Z}^3$ is the pixel color at (x, y) . In particular, $v = f(x, y)$ where $v = (r, g, b)$ is a color and for any k bits $r, g, b \in \{0, 1, \dots, 2^k - 1\}$ is the component intensity of the corresponding *R*, *G* and *B*, respectively. The $f(x, y)$ is the resulting color of the component mixture at pixel (x, y) for an *RGB* color image. The intensity of each component is usually normalized, i.e. $r, g, b \in [0, 1]$. The set of colors v is denoted by Ω .

A structure for ordering in the set of Ω is defined through a homogeneous binary relation. i.e. an endorelation over Ω denoted by \mathcal{R} , such that the binary relation on a set Ω is defined as a collection of ordered pairs of elements

of Ω specified by $v\mathcal{R}w$ meaning that v is \mathcal{R} -related to w . A binary relation \mathcal{R} on a set Ω is called:

- 1) Reflexive if $v\mathcal{R}v, \forall v \in \Omega$,
- 2) Antisymmetric if $v\mathcal{R}w \wedge w\mathcal{R}v \Rightarrow v = w, \forall v, w \in \Omega$,
- 3) Transitive if $v\mathcal{R}w \wedge w\mathcal{R}z \Rightarrow v\mathcal{R}z, \forall v, w, z \in \Omega$,
- 4) Total if $w \leq v \vee v \leq w, \forall v, w \in \Omega$.

If the binary relation satisfies expressions (1) and (3) is called a *pre-ordering* relation. If, in addition, it satisfies the expressions (2) is called as an *ordering* relation and if in addition expression (4) is satisfied, the binary relation is called as *total*, otherwise it is called *partial*. In this work a new ordering relation is established, denoted by $\hat{\mathcal{R}}$. For this, it is presented a new transformation that produces an ordering which avoids any arbitrary criterion to assign a higher priority to any of the three color components. To this end, a transformation $\mathcal{T} : \mathbb{Z}^3 \rightarrow \mathbb{R}$ is defined, and then the colors are ordered according to the scalar order.

A color reduction transformation is defined as $\mathcal{T} : f(x, y) \rightarrow \mathbb{R}$ by the inner product of color v and a weighted vector $\psi = (\psi_1, \psi_2, \psi_3)$ as follows:

Definition 1: Let $v = (r, g, b)$ be an RGB color, and $\psi = (\psi_1, \psi_2, \psi_3)$ a weighted vector such that $\psi \in \mathbb{R}^3$, then the transformation \mathcal{T} is defined by the inner product expression:

$$\mathcal{T}(v) := \langle v, \psi \rangle. \quad (1)$$

For defining more appropriately the transformation \mathcal{T} , the histogram of j -th color component associated to a specific region in the image, denoted by $\mathcal{D}_m \subset \mathcal{D}$, where the subindex m denotes any subregion in the image, is defined as $h_{f_j}^{\mathcal{D}_m}(i) := n_i$, where i represents the i -th level of intensity in the range $\{0, 1, \dots, 2^k - 1\}$ of component j -th, and n_i is the number of pixels in image f , whose intensity level is i in component j -th within domain \mathcal{D}_m (subset of pixels (x, y) in the image f).

The values of ψ are obtained by applying function $\phi \in \mathbb{R}$ over each component histogram in the domain \mathcal{D}_m of image f . In the context of this paper, the function ϕ is obtained through the application of a statistical function to each R, G , and B component histogram, $\psi_1 = \phi(h_{f_1}^{\mathcal{D}_m})$, $\psi_2 = \phi(h_{f_2}^{\mathcal{D}_m})$, $\psi_3 = \phi(h_{f_3}^{\mathcal{D}_m})$. This is done in order to give more weight to the component whose statistical parameter has the highest value in domain $\mathcal{D}_m \subset \mathcal{D}$ (this could be the whole image or part of it). The partition of the domain \mathcal{D} for obtaining the subdomain \mathcal{D}_m is considered latter (see the next subsection).

The following functions ϕ were applied to each component j of image f in all the tests:

- Mean (ϕ_{Me}): the sum of all intensity levels i that appear in domain \mathcal{D}_m divided by the pixel quantity n in \mathcal{D}_m :

$$\phi_{Me}(h_{f_j}^{\mathcal{D}_m}) = \sum_{i=0}^{2^k-1} \frac{i \times h_{f_j}^{\mathcal{D}_m}(i)}{n}, \quad (2)$$

where $n = n_0 + n_1 + \dots + n_{2^k-1}$.

- Minimum (ϕ_{Min}): the lowest intensity level i in domain \mathcal{D}_m :

$$\phi_{Min}(h_{f_j}^{\mathcal{D}_m}) = \min\{i | h_{f_j}^{\mathcal{D}_m}(i) > 0\}. \quad (3)$$

- Maximum (ϕ_{Max}): the highest intensity level i in domain \mathcal{D}_m :

$$\phi_{Max}(h_{f_j}^{\mathcal{D}_m}) = \max\{i | h_{f_j}^{\mathcal{D}_m}(i) > 0\}. \quad (4)$$

- Minimum Mode (ϕ_{minM_o}): the lowest intensity level i that appears the most times in domain \mathcal{D}_m :

$$\phi_{minM_o}(h_{f_j}^{\mathcal{D}_m}) = \min\{i | h_{f_j}^{\mathcal{D}_m}(i) \geq h_{f_j}^{\mathcal{D}_m}(i'), \forall i \neq i'\}. \quad (5)$$

- Maximum Mode (ϕ_{maxM_o}): the highest intensity level i that appears the most times in domain \mathcal{D}_m :

$$\phi_{maxM_o}(h_{f_j}^{\mathcal{D}_m}) = \max\{i | h_{f_j}^{\mathcal{D}_m}(i) \geq h_{f_j}^{\mathcal{D}_m}(i'), \forall i \neq i'\}. \quad (6)$$

- Variance (ϕ_{Var}): the intensity level variance in domain \mathcal{D}_m :

$$\phi_{Var}(h_{f_j}^{\mathcal{D}_m}) = \sum_{i=0}^{2^k-1} \frac{h_{f_j}^{\mathcal{D}_m}(i) \times (i - \phi_{Me}(h_{f_j}^{\mathcal{D}_m}))^2}{n}. \quad (7)$$

- Smoothness(ϕ_R): measurement of the relative smoothness of the intensity in domain \mathcal{D}_m :

$$\phi_R(h_{f_j}^{\mathcal{D}_m}) = 1 - \frac{1}{1 + \phi_{Var}(h_{f_j}^{\mathcal{D}_m})}. \quad (8)$$

The induced Reduced ordering (\mathcal{R} -ordering) of the transformation \mathcal{T} consists in reducing the color vectors v and v' to a scalar values using its respective transformations $\mathcal{T}(v)$ and $\mathcal{T}(v')$, and then rank them in accordance to the scalar ordering. In this paper, we consider the induced \mathcal{R} - binary relation with respect to the transformation (1) as:

Definition 2: Let v and v' be two colors in the set of colors Ω on a subdomain $\mathcal{D}_m \subset \mathcal{D}$. An ordering relation, denoted by \mathcal{R} - binary relation is defined by the following implication:

$$\forall v, v' \in \Omega, \quad \mathcal{T}(v) \leq \mathcal{T}(v') \Rightarrow v \leq_{\mathcal{R}} v'. \quad (9)$$

The characterization of the properties of the implication (9) in terms of the reflexive and transitive properties is given in the following Lemma.

Lemma 1: Consider the \mathcal{R} - binary relation in the subdomain $\mathcal{D}_m \subset \mathcal{D}$, the transformation \mathcal{T} defined by expression (1) and two colors v and v' associated with the pixels (x, y) and (x', y') , then the \mathcal{R} - binary relation $\mathcal{T}(v) \leq \mathcal{T}(v') \Rightarrow v \leq_{\mathcal{R}} v'$ is reflexive and transitive.

Proof: Reflexive $v\mathcal{R}v$. Let v be a color associated with a pixel $(x, y) \in \mathcal{D}_m$, then $\mathcal{T}(v) \leq \mathcal{T}(v)$, $\mathcal{T}(v) = q, q \in \mathbb{R}$. Since $q \leq q$, therefore $v \leq_{\mathcal{R}} v$, and consequently the \mathcal{R} -binary relation is reflexive.

Transitive $v\mathcal{R}v' \wedge v'\mathcal{R}v'' \Rightarrow v\mathcal{R}v''$. Let v, v' and v'' colors associated with pixels $(x, y), (x', y')$ and $(x'', y'') \in \mathcal{D}_m$, and considering $\mathcal{T}(v) = q, q \in \mathbb{R}, \mathcal{T}(v') = q', q' \in \mathbb{R}$ and $\mathcal{T}(v'') = q'', q'' \in \mathbb{R}$, then the expression $\mathcal{T}(v) \leq \mathcal{T}(v') \wedge \mathcal{T}(v') \leq \mathcal{T}(v'')$ can be reduced to $q \leq q' \wedge q' \leq q''$, which implies that $q \leq q''$ and therefore $v \leq_{\mathcal{R}} v''$ (consequently the \mathcal{R} -binary relation is transitive). \square

Observe that since the \mathcal{R} - binary relation is reflexive and transitive, it is a pre-ordering relation. A problem with the

\mathcal{R} - binary relation induced by the transformation (1) can lead to a non - injective transformation, i.e., given two different colors v and v' associated to two different pixels (x, y) and (x', y') , respectively; it is desirable that the transformation assures $\mathcal{T}(v) \neq \mathcal{T}(v')$ for $v \neq v'$. Unfortunately, depending on the transformation this desirable property could not be obtained, and it can be that $\mathcal{T}(v) = \mathcal{T}(v')$. The following Lemma shows this situation:

Lemma 2: Given two different colors v and v' be in the subdomain $\mathcal{D}_m \subset \mathcal{D}$, and the weighted vector ψ , such that $\psi \in \mathbb{R}^3$. There exists a set of ψ_l such that $\mathcal{T}(v) = \mathcal{T}(v')$

Proof: In order of having, $\mathcal{T}(v) = \mathcal{T}(v')$ and assuming that ψ and v' are given, we have:

$$\langle v, \psi \rangle = \langle v', \psi \rangle. \quad (10)$$

Hence the linear equation (10) has a bi-dimensional Kernel \mathcal{K} , and consequently, infinite vectors v (not necessarily equals to v') satisfies the equation (10). \square

By the Lemma 2, the \mathcal{R} - binary relation is not injective and consequently, the antisymmetric property is not satisfied.

At this point, we are interested in having an ordering relation in the set of color Ω associated to each sub-domain \mathcal{D}_m and transform the \mathcal{R} - binary relation in an injective one. To this end, let consider an extended color vector \hat{v} defined as $\hat{v}_1 = \mathcal{T}(v)$ and $\hat{v}_l = v_{l-1}$ for all $l \geq 2$.

Definition 3: Let v and v' be two colors in the set of colors Ω on a subdomain $\mathcal{D}_m \subset \mathcal{D}$. A lexicographical ordering relation, denoted by $\hat{\mathcal{R}}$ - binary relation is defined by the following implication:

$$\forall v, v' \in \Omega, \quad \hat{v} \leq_L \hat{v}' \Rightarrow v \leq_{\hat{\mathcal{R}}} v' \quad (11)$$

where \leq_L indicates the relation \leq according to the lexicographical ordering.

In the next Theorem, it is formalized important properties of the proposed $\hat{\mathcal{R}}$ - binary relation.

Theorem 1: The ordering between colors v and v' is a total order under the $\hat{\mathcal{R}}$ - binary relation of Definition 3.

Proof: It is straightforward from considering that the lexicographical order (\leq_L) is a total order and $\hat{v} \leq_L \hat{v}' \Rightarrow v \leq_{\hat{\mathcal{R}}} v'$ then $\hat{\mathcal{R}}$ ordering ($\leq_{\hat{\mathcal{R}}}$) is also a total order. \square

After the transformation \mathcal{T} , the priority of the color components could be changed in the extended color vector. The main idea behind the consists in giving higher priority to the transformation \mathcal{T} with respect to the higher priority of the component whose statistical parameter is higher, according to the function ϕ associated to the region \mathcal{D}_m analyzed.

A direct consequence of the statement above is the need of an appropriate partition of the domain \mathcal{D} in subdomains \mathcal{D}_m , since the subdomains affects the computation of the weights ψ_l and the transformation \mathcal{T} . In this work, two domain partition strategies are explored: 1) partition based on neighborhood and 2) partition the image into sub-regions. Other criteria can be used which yield other kind of partition. The exploration of partitions is left as a future work.

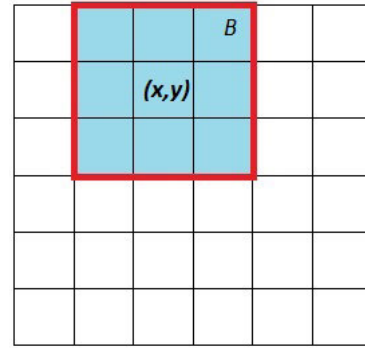


FIGURE 1. Neighborhood B of size 3×3 centered at pixel (x, y) .

A. DOMAIN PARTITION STRATEGIES

We need to define the domain $\mathcal{D}_m \subset \mathcal{D}$ to calculate the weights ψ_l . The function ϕ is applied to each histogram of the color component ($h_{f_j}^{\mathcal{D}_m}$) in domain \mathcal{D}_m .

1) FIRST STRATEGY: PARTITION BASED ON NEIGHBORHOOD

Given a color image f and a filter F , the application of F to f can be expressed as $g(x, y) = F\{f(x, y)\}$, where (x, y) represents a pixel for a specific color v and g is the filtered image. Order filters are nonlinear neighborhood operations, where a function is applied to the neighborhood of each pixel. The idea is to move a window B through the entire image. This window B is centered on each pixel and get a new value, which is the result of selecting one pixel from all previously ordered pixels in the window. For example, a pixel in the new image may be the result of getting the median, minimum, or maximum of the colors ordered in B .

\mathcal{D}_m is the B window (called the structuring element in the mathematical morphology (see the next subsection)), where the operation (order filter) is applied. Figure 1 depicts a domain \mathcal{D}_m corresponding to a neighborhood B of size 3×3 centered in the pixel (x, y) .

2) SECOND STRATEGY: PARTITION THE IMAGE INTO SUB-REGIONS

In order to obtain local information from an image f , it is divided into λ sub-regions $\{W_l\}$, $l = \{1, \dots, \lambda\}$. Let B be a window or a structuring element, and \mathcal{D}_m its corresponding domain centered at pixel (x, y) . Then any region in contact with a pixel of B is considered as part of \mathcal{D}_m .

Figure 2 depicts the image division into four sub-regions: W_1 , W_2 , W_3 , and W_4 . The region delimited by window B is shaded. The domain \mathcal{D}_m used to compute the weights ψ_l using B represents the zone corresponding to sub-region W_1 .

It should be noted that the window will not necessarily be included in a single sub-region. Because the window moves through the entire image, it may touch more than one sub-region. Figure 3 depicts a domain \mathcal{D}_m , where the weights will be calculated. Domain \mathcal{D}_m belongs to the union of

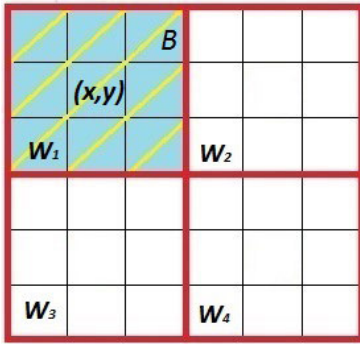


FIGURE 2. Domain when window is in contact with one sub-region.

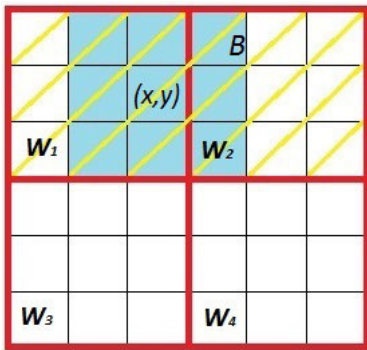


FIGURE 3. Domain when window is in contact with more than one sub-region.

sub-regions W_1 and W_2 , and window B is in contact with both sub-regions. This ensures that the weighted vector ψ will be the same for all pixels in B . Thus, when two different pixels are to be compared with the same color v , the same transformation \mathcal{T} can be obtained.

In this context, we can consider the global information as a special case in which the image is not split into regions so that the region is the full image. In this case the weights are computed from the entire image.

In our tests, input images with a size of $M \times N$ pixels were divided into sub-regions $W_{\{1,2,\dots,\lambda\}}$ with $\lfloor \frac{M}{M'} \rfloor$ rows and $\lfloor \frac{N}{N'} \rfloor$ columns, where $\lfloor \cdot \rfloor$ indicates the floor function. In this way, we obtained a new matrix with M' rows and N' columns, whose element was sub-region W_l .

Note that since the $\hat{\mathcal{R}}$ - binary relation depends on the selection of the weighted vector and the domain \mathcal{D}_m , from which the statistical parameters are extracted as components of that vector, it is possible to have an ordering framework. In the ordering framework you can configure different domain partition strategies with different statistical parameters depending on the type of image to be treated or the application. In the Figure 4 it can be observed the flow chart of the ordering framework. It should be noted that the sequence of steps shown in the flow chart must be applied in the filter window for each pixel within the image.

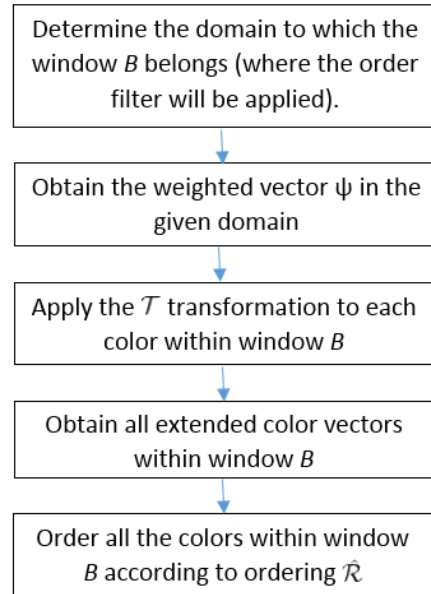


FIGURE 4. Flow chart of the ordering framework.

B. MATHEMATICAL MORPHOLOGY

Mathematical morphology as a particular case of order filtering is based on two basic operators: erosion and dilation. Such operators can be defined by the minimum and maximum within a special window B called a structuring element. Given a digital image f and structuring element B ; the erosion (ε) and dilation (δ) of image f for all pixels (x, y) with respect to B are defined as follows:

$$\varepsilon(f, B)(x, y) = \min\{f(x - s, y - t), \forall (s, t) \in B\}, \quad (12)$$

$$\delta(f, B)(x, y) = \max\{f(x + s, y + t), \forall (s, t) \in B\}. \quad (13)$$

The combination of erosion and dilation produces other operators such as opening and closing. The opening \circ and closing \bullet of f by B are defined based on the dilation and erosion as follows:

$$f \circ B = \delta(\varepsilon(f, B), B), \quad (14)$$

$$f \bullet B = \varepsilon(\delta(f, B), B). \quad (15)$$

In practice, opening smooths the bright regions of the image. Closing smooths the dark zones of the image. An operator is considered morphological if it has some properties such as anti-extensive or extensive, idempotent, homotopy, and increasing [47].

The extension of mathematical morphology for color images remains an open problem [48], mainly because there is no a natural order between colors. In the RGB color image, the priority of the color component is given by the ordering when applying a filter over the image using the lexicographical ordering. However, the same ordering filter may yield to different results depending on which component is prioritized. Figure 5 depicts an example of the application of the dilatation operator with a square structuring element B (size 3×3) to a synthetic color image (Figure 5(a)) using the

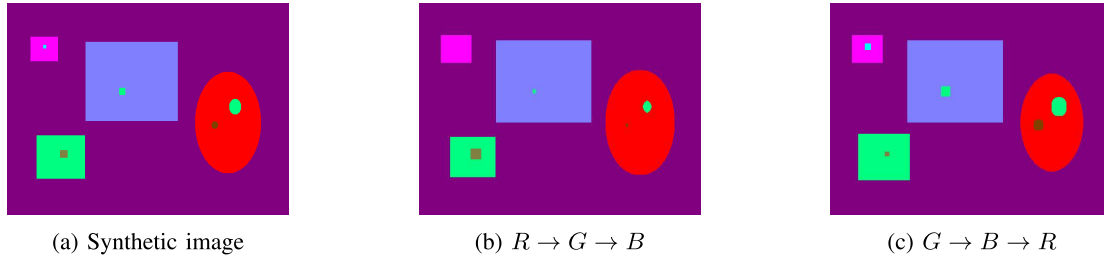


FIGURE 5. Example of applying the dilation operator to a synthetic image.

lexicographical ordering $R \rightarrow G \rightarrow B$ and $G \rightarrow B \rightarrow R$. In the image in Figure 5(b), it can be observed how the green objects decrease in size and the red object size increases. In the image of Figure 5(c) occurs exactly the opposite. This is because the red component has a higher priority in ordering in Figure 5(b), while the green component has a higher priority in Figure 5(c). This simple example shows the importance of choosing adequately the component priority in the lexicographical ordering. In fact, this prioritization is highly dependent on the type of image or application.

III. APPLICATIONS

In this paper, two applications are shown. The first one is noise reduction and the second is contrast enhancement using mathematical morphology.

For the examples in this section and in the experiments (next section), we use the following abbreviations:

- *ED*: The Euclidean norm in *RGB* was used as the color ordering method [11].
- *BM*: Bit mixing ordering in *RGB* was used as the color ordering method [45].
- *LEX*: Lexicographical ordering in *RGB* was used as the color ordering method.
- *ALEX*: α -lexicographical ordering in *RGB* [49] was used for color ordering. The value of $\alpha = 10$.
- *AMLEX*: α -module lexicographical ordering in *RGB* [31] was used for color ordering. The value of $\alpha = 10$.
- *HLEX*: $I \rightarrow S \rightarrow H$ lexicographical ordering was used for color ordering.
- *DLAB*: The Euclidean norm in $L^*a^*b^*$ was used as the ordering method [11].
- *OL*: An ordering method based on the ordering of Loewner [24].
- *MIN*: Equation 1 was used to add this transformation as the initial element to the extended color vector, where: $\psi = (\phi_{Min}(h_{f_1}^{D_m}), \phi_{Min}(h_{f_2}^{D_m}), \phi_{Min}(h_{f_3}^{D_m}))$.
- *MAX*: Equation 1 was used to add this transformation as the initial element to the extended color vector, where: $\psi = (\phi_{Max}(h_{f_1}^{D_m}), \phi_{Max}(h_{f_2}^{D_m}), \phi_{Max}(h_{f_3}^{D_m}))$.
- *MO1*: Equation 1 was used to add this transformation as the initial element to the extended color vector, where: $\psi = (\phi_{minM_o}(h_{f_1}^{D_m}), \phi_{minM_o}(h_{f_2}^{D_m}), \phi_{minM_o}(h_{f_3}^{D_m}))$.

- *MO2*: Equation 1 was used to add this transformation as the initial element to the extended color vector, where: $\psi = (\phi_{maxM_o}(h_{f_1}^{D_m}), \phi_{maxM_o}(h_{f_2}^{D_m}), \phi_{maxM_o}(h_{f_3}^{D_m}))$.
- *SMO*: Equation 1 was used to add this transformation as the initial element to the extended color vector, where: $\psi = (\phi_R(h_{f_1}^{D_m}), \phi_R(h_{f_2}^{D_m}), \phi_R(h_{f_3}^{D_m}))$.
- *MEAN*: Equation 1 was used to add this transformation as the initial element to the extended color vector, where: $\psi = (\phi_{Me}(h_{f_1}^{D_m}), \phi_{Me}(h_{f_2}^{D_m}), \phi_{Me}(h_{f_3}^{D_m}))$.
- *VAR*: Equation 1 was used to add this transformation as the initial element to the extended color vector, where: $\psi = (\phi_{Var}(h_{f_1}^{D_m}), \phi_{Var}(h_{f_2}^{D_m}), \phi_{Var}(h_{f_3}^{D_m}))$.

A. NOISE REDUCTION

In images, noise is a random variation of brightness or color information due to capture, storage, transmission, processing, or conversion [50]. From the theoretical point of view, several mathematical models have been developed to generate different types of noise.

Let f' be the result of contaminating image f with a certain type of noise, with vector $\eta = (\eta_1, \eta_2, \eta_3)$, in which each element in η corresponds to a random variable. The utilized noise models are defined as follows:

- *Gaussian noise*: This is an additive statistical noise with a density function of Gaussian probability [51]. Gaussian noise is expressed as follows:

$$f'(x, y) = f(x, y) + \eta, \quad (16)$$

where each component η_l is a random variable with a normal distribution, average μ , and variance σ^2 .

- *Speckle noise*: This is a multiplicative statistical noise with a uniform probability density function, defined as follows:

$$f'(x, y) = f(x, y) + \eta * f(x, y), \quad (17)$$

where the operator $*$ symbolizes the Hadamard product (element to element). Each element η_l is a uniformly distributed random value with an average μ and variance σ^2 .

Figure 6 depicts an untouched image (6(a)), and the same image after adding noise (6(b-c)) The noise parameters are ($\sigma^2 = 0.105, \mu = 0$) for the Gaussian noise and ($\sigma^2 = 0.05, \mu = 0$) for the speckle noise.

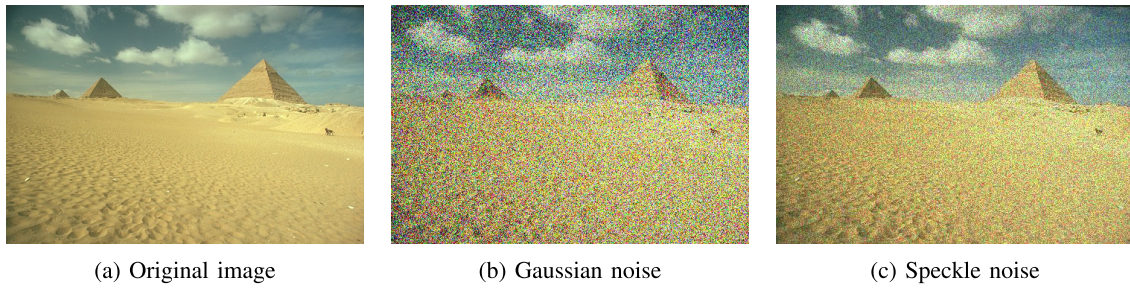


FIGURE 6. Image with different types of noise.

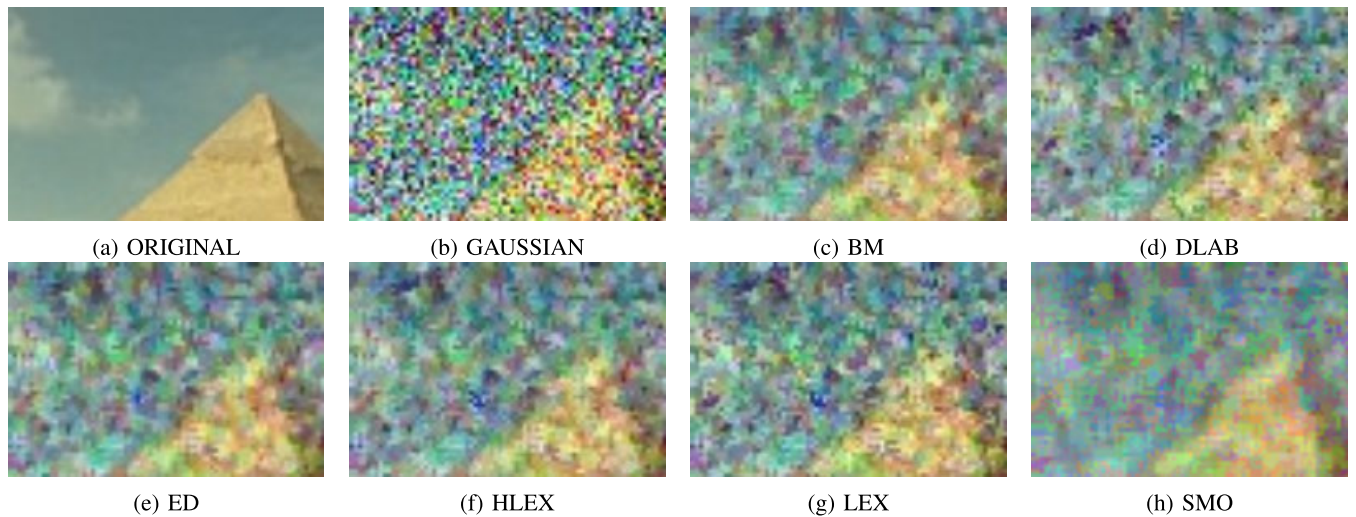


FIGURE 7. Results from applying different filters. The image was divided into 5 × 5 sub-regions.

In order to establish which ordering method is more efficient for noise reduction, the images resulting from applying the median filter with different ordering methods to a noisy image should be compared. In this case, the median filter is applied to the image contaminated with Gaussian noise (Figure 6(b)). One of the objectives when working with image filtering regardless of the noise present is to have a good balance between image smoothing and edge preservation. The ideal filter for image enhancement is one that is capable of preserving fine edges and details. Some filters, by reducing noise, inevitably eliminate a considerable amount of detail.

Figure 7 depicts the results of the median filter using different ordering methods in the tip of the pyramid. The idea is to compare the visual results obtained by the different ordering methods using the same filter, and thus observed, which results are the closest to the original image and is capable of preserving fine edges and details.

The methods proposed in the literature are very similar visually, in the sense that they reduce noise, but the results are not so smooth, and do not maintain the structure of the pyramid (eliminate a considerable amount of detail). The results of using the ordering methods in the $L^*a^*b^*$ and HSI color spaces are shown. In the RGB color space the BM and ED methods are shown, and of all lexicographical

methods only the LEX method is shown (Figure 7(c-g)). The images filtered using the proposed ordering and different weights are visually better than those methods proposed in the literature (the resulting image maintains the structure of the pyramid and is much smoother). They also are perceptually very similar to each other, getting a good balance between image smoothing and edge preservation. Figure 7(h) depicts the filter results using of method SMO .

B. CONTRAST ENHANCEMENT USING MATHEMATICAL MORPHOLOGY

Based on opening and closing, other operators such as top-hat (TH) and bottom-hat (BH) are defined as follows:

$$TH(f) = f - f \circ B, \tag{18}$$

$$BH(f) = f \bullet B - f. \tag{19}$$

The advantages of using TH and BH are the possibilities of extracting small bright and dark sets in complex contexts, respectively [52], [53]. Operators with the proposed order are not purely morphological because theoretical properties such as idempotent cannot be guaranteed for opening and closing. Because the information extracted in the form of weights (as a result of applying a function ϕ) can be different, a color

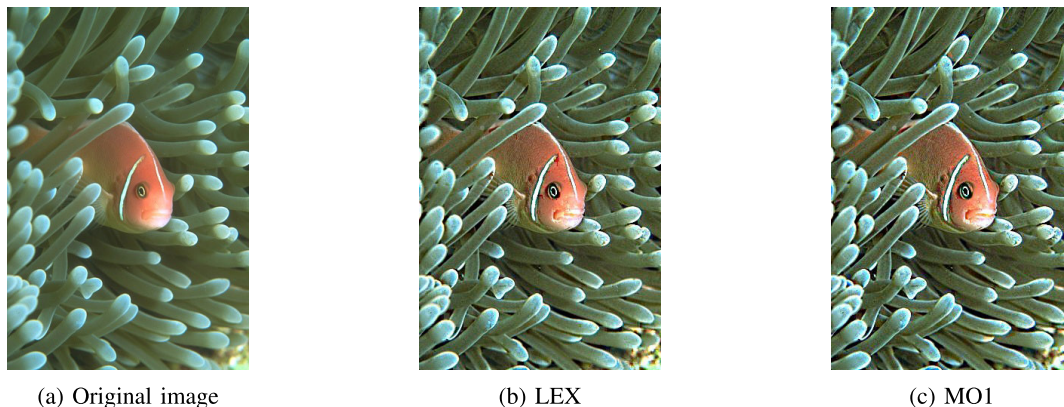


FIGURE 8. Visual result of applying contrast enhancement.

can be considered higher or lower than another color in a domain D but not in another one.

Even when using the same domain, the weights can vary in the next iteration (as a consequence of reapplying the same operator), because the information extracted varies from one iteration to another. In the literature, this kind of operator is called a pseudo-operator [19]–[21], [48], [54].

A contrast enhancement strategy [46] consists of adding bright regions to (TH) and subtracting dark ones (BH) from image f as follows:

$$MC(f) = f + TH(f) - BH(f), \quad (20)$$

where $MC(f)$ is the contrast enhancement of f .

In order to increase the bright regions and decrease the dark parts of an image, in this work we propose to generalize the expression proposed in [46] by adding the weight β so that:

$$MC(f) = f + \beta \times TH(f) - \beta \times BH(f). \quad (21)$$

This factor affects the contrast so that increasing β implies a higher contrast.

Figure 8 presents the visual results of applying contrast enhancement with ordering methods LEX and $MO1$ to an image (Figure 8(a)). We can see that both methods enhance the contrast in relation to the original image. Our method $MO1$, unlike the LEX method, not only generates less distortion, but also improves the details of the image. The difference between the different ordering methods in both applications is shown in the numerical results discussed later in the next section.

IV. EXPERIMENTAL RESULTS

This section presents the different experiments performed to evaluate the proposed framework. Such experiments are divided into two parts:

- 1) In the first part (Section IV-A), we evaluate the performance of the proposal in the presence of noise.
- 2) In the second part (Section IV-B), we assess the proposal in the contrast enhancement application. In this case the contrast enhancement is done using

the morphological method presented previously (see equation 21).

The proposed framework was compared with the following popular ordering methods: classical lexicographical ordering, α -lexicographical ordering [49], α -module lexicographical ordering [31], $I \rightarrow S \rightarrow H$ lexicographical ordering, ($Href = 0\check{A}\check{Z}$) [32], bit-mixing [45], the Euclidean distance to color (0, 0, 0) method in the $L^*a^*b^*$ and RGB color spaces [11], and an ordering method based on the ordering of Loewner [24]. The same abbreviations used in the previous section were used for differentiation of ordering methods.

A. NOISE REDUCTION

The objective of this experiment is to compare the ordering methods in noisy images after applying a well known filter to reduce noise as the median.

In order to evaluate the filter efficiency with different ordering, we used the mean absolute error to measure how close the predictions were to the actual observations [55]. Given an image f and its filtered image g with the dimensions $M \times N$, the mean absolute error of the filtered image is given by:

$$MAE(f, g) = \frac{1}{3 \times M \times N} \sum_{j=1}^3 d_j, \quad (22)$$

where:

$$d_j = \sum_{\substack{x \in \{1, \dots, M\} \\ y \in \{1, \dots, N\}}} |[f(x, y)]_j - [g(x, y)]_j| \quad (23)$$

We used 100 different images from [56], polluted with Gaussian and speckle noise. It is worth mentioning that the input images were normalized at interval [0, 1] to generate the noise, and then changed again to their original interval [0, 1, ..., $2^k - 1$] ($k = 8$) for the filter applications and subsequent evaluations. For both speckle and Gaussian noise, the value of μ was set to 0 while σ^2 varied between 0.005 and 0.165, in increments of 0.01.

For each noise type we evaluate the goodness of the proposal by performing the following experiments:

- 1) First, we test how changes the values when varying the window size with the methods from the literature.
- 2) Then, we perform similar experiments to previous one, but now varying number of sub-regions (Second strategy) and the window size (First strategy) with the proposal.
- 3) We continue comparing the proposal with the best configuration of window size, number of sub-regions and other ordering methods.
- 4) Finally, we present a ranking of the different methods used with the best parameter values. This ranking is presented for different noise levels.

The results in this section differentiate the order filters of each weight (obtained by applying the ϕ function) according to their domain partition. As a reference, a suffix *WX* was added to the designations of the proposed filters, where *X* represents the number of sub-regions in which the image was divided. If *X* is equal to 0 (zero), the neighborhood (marked by the filter window) is the domain (first strategy). In order to distinguish the size of the window, suffix *B* is used before suffix *WX*. For instance, *B3W0* implies that a 3×3 window was used by the neighborhood as the domain. Similarly, *B5W9* implies that a 5×5 window was used, and the image was divided into 9 sub-regions of the same size.

1) WINDOW SIZE ANALYSIS

The objective of the analysis is to determine which filter window sizes are best suited to reduce noise for different ordering methods in the literature. The horizontal axis (or abscissa) is assigned the window size values (B3, B5 and B7) and the vertical axis or ordinate is assigned the values of the MAE metric as B increases for each ordering method. As shown in Figure 9, it can be seen that the size of the B filter window is more important than the ordering methods.

Figure 9 depicts that in comparison to the 3×3 window for Gaussian noise, better results could be obtained with 5×5 and 7×7 windows on average, with σ^2 values between 0.005 and 0.165 (17 in total \times 100 images) for the methods proposed in the literature. Method *ED* gave better results than the rest, while method *BM* remained in second place. The *OL* method performed worse than the other methods.

Figure 10 depicts the filter results with the ordering methods proposed in the literature, for speckle noise. We can see that a smaller window size provides better average results. In addition, *ED* is the method with the best performance and *OL* is the method with the worst performance.

2) NUMBER OF SUB-REGIONS AND THE WINDOW SIZE (STUDY)

The objective of the analysis is to determine which numbers of sub-regions and window sizes in the framework are best suited for noise reduction. The horizontal axis (or abscissa) is assigned the values of window size B and the number of subregions W. The vertical axis (or ordinate) is assigned the values of the MAE metric for each ordering method.

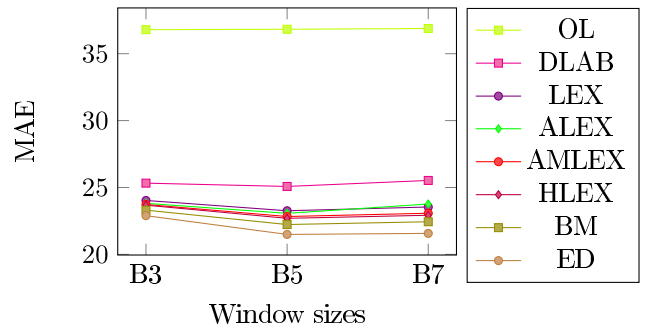


FIGURE 9. Gaussian noise. Average MAE of 1700 images (100 x 17) per window size. Proposed methods in literature.

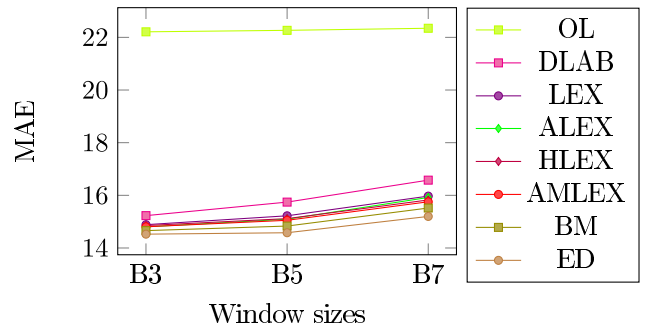


FIGURE 10. Speckle noise. Average MAE of 1700 images (100 x 17) per window size. Proposed methods in literature.

Figure 11 depicts the behavior of the Gaussian noise filter using different domain partitions for the proposed ordering. Every curve presents the same form, i.e., the filters present the same relative behavior regarding the domain partition. Better average results were obtained for the 5×5 and 7×7 windows in comparison to the 3×3 window (just as occurred with the methods proposed in the literature). It is also noticeable that the domain was not as important as the weights. The neighborhood was better as a domain than the division into sub-regions for methods *MIN*, *MO1*, and *MO2*. These 3 methods were the ones with the worst results. On the other hand, *VAR*, *SMO*, *MAX*, and *MEAN* had better results, and were practically equal regardless of the domain used for the weight calculations.

Figure 12 depicts the filter behavior for speckle noise, when using different domain partitions with the framework. Every curve presents the same form. In other words, the filters present the same relative behavior regarding the domain partition. We can see that the domain is not very important, except in *MIN*, where the results vary depending on the way the domain is distributed. In addition, in relation to the weights, the methods with the best results are *MAX* and *SMO*.

3) ORDERING METHODS COMPARISON

For each statistical parameter and noise, a graph of the trend curves of each filter in relation to the noise variation parameter (σ^2) is presented. Each point represents the average of the results for 100 images from the database [56] obtained by that filter for a certain noise parameter value (σ^2 , MAE).

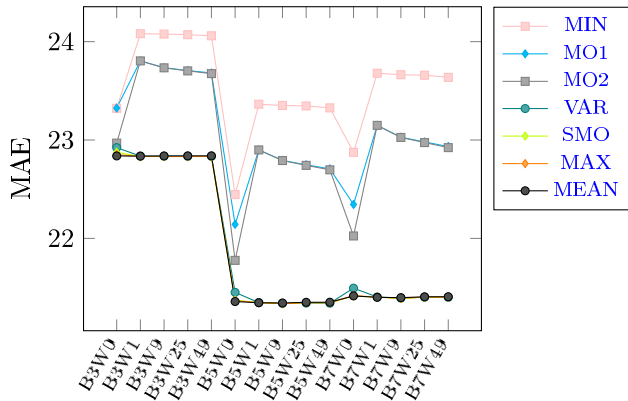


FIGURE 11. Gaussian noise. Average MAE of 1700 images by domain partition. Proposed filters.

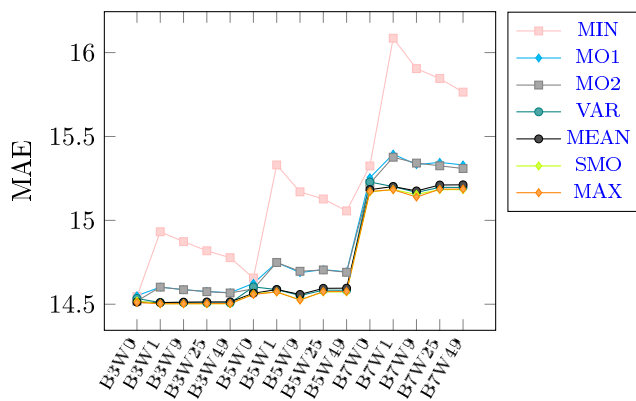


FIGURE 12. Speckle noise. Average MAE of 1700 images by domain partition. Proposed filters.

The curve corresponding to a filter was obtained by joining each pair of successive points of said filter with the straight line passing through both points.

Figure 13 depicts the behavior of the Gaussian noise filter (with the best configuration by ordering method) with the increase of σ^2 . The horizontal axis (or abscissa) is assigned the value of σ^2 and the vertical axis (or ordinate) is assigned the MAE values of the different ordering methods as σ^2 increases. The goal is to display the MAE values as the noise increases. It can be seen that the MAE values increase as σ^2 increases.

We can see that the framework with all the weights is better than the methods proposed in the literature for almost every point (with the exception of the initial points). *MEAN*, *MAX*, and *SMO* were the 3 best methods, with practically the same results. The *OL* method was worse in performance than the other methods for all σ^2 value. This can be seen in the legends of the box on the right of the Figure, where the methods are ordered according to their MAE value from highest to lowest. The ordering methods resulting from the use of the framework are painted in blue.

Figure 14 depicts each filter behavior for speckle noise (with their best configuration) with an increase in σ^2 . We can see that the framework, for most weights, is better than those proposed in the literature. Once again, *ED* is the best method

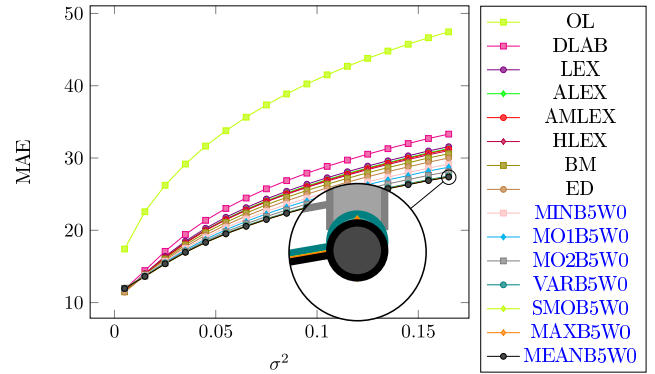


FIGURE 13. Gaussian noise. MAE average of 100 images by σ^2 . Best configurations.

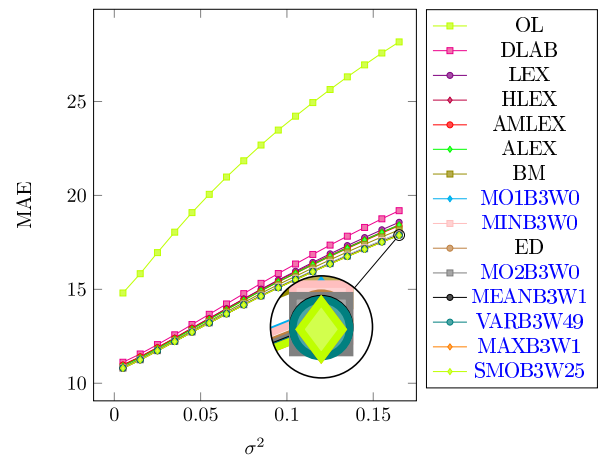


FIGURE 14. Speckle noise. MAE average of 100 images by σ^2 . Best configurations.

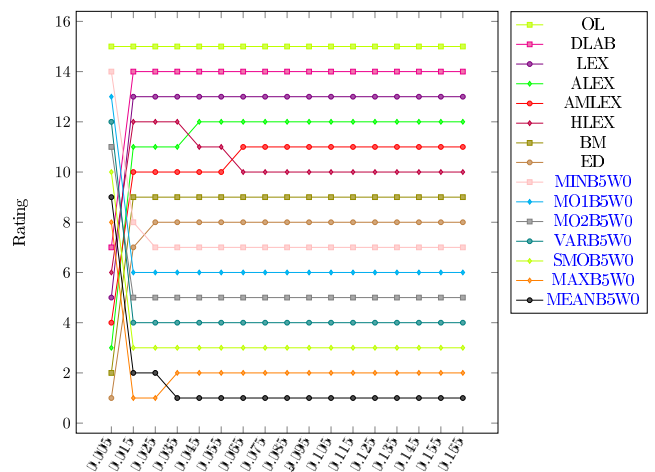


FIGURE 15. Gaussian noise. Ranking.

among those proposed in the literature and *OL* is the method with the worst performance.

4) RANKING THE ORDERING METHODS

Figure 15 depicts the ranking (order axis) as σ^2 increases (abscissa axis). Lower values for *MAE* imply better ranking positions. It is noticeable that when σ^2 is equal to 0.015,

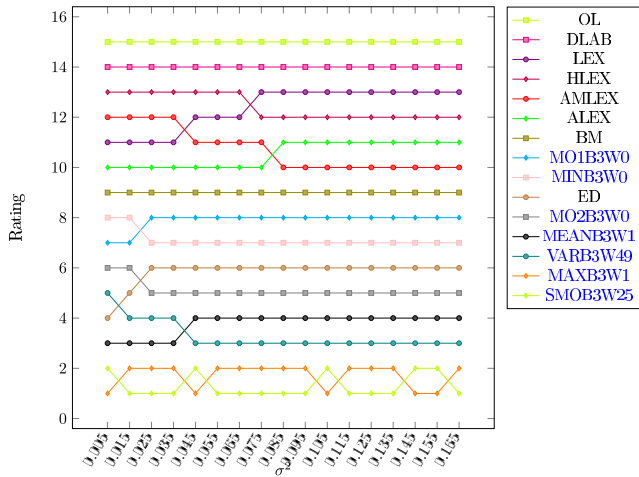


FIGURE 16. Speckle noise. Ranking.

the framework with different weights gives better results than the methods proposed in the literature. This shows that with higher noise, the framework, with any of the weights, gives better results than the other methods with Gaussian noise.

Figure 16 depicts that, in the speckle noise ranking, all of the methods are stable even if the noise increases, with very few jumps. Method *ED* started with the 4th position and ended with the 6th. It was surpassed by *MO* and *VAR*, which started from σ^2 equal to 0.025.

B. CONTRAST ENHANCEMENT

We may assess the contrast enhancement effectiveness using a method called the contrast improvement ratio (*CIR*), which quantifies the level of image contrast enhancement [57]. The local contrast $c(x, y)_j$ for component j is defined as follows:

$$c(x, y)_j = \left| \frac{\rho - a}{\rho + a} \right|, \tag{24}$$

where ρ is the intensity of component j in (x, y) , and a is the average intensity of the eight neighbors in a 3×3 matrix of pixels centered on (x, y) .

The performance measure CIR_j is defined as the ratio of the enhanced image and original image for each component j .

$$CIR_j = \frac{\sum_{(x,y)} |c(x, y)_j - \check{c}(x, y)_j|^2}{\sum_{(x,y)} c(x, y)_j^2}, \tag{25}$$

where c and \check{c} are the local contrast values of the original image and the enhanced one, respectively.

The performance measure *CIR* is defined as follows:

$$CIR = \frac{1}{3} \sum_{j=1}^3 CIR_j. \tag{26}$$

The tests were performed using a database composed of 100 images [56]. The structuring element is an important

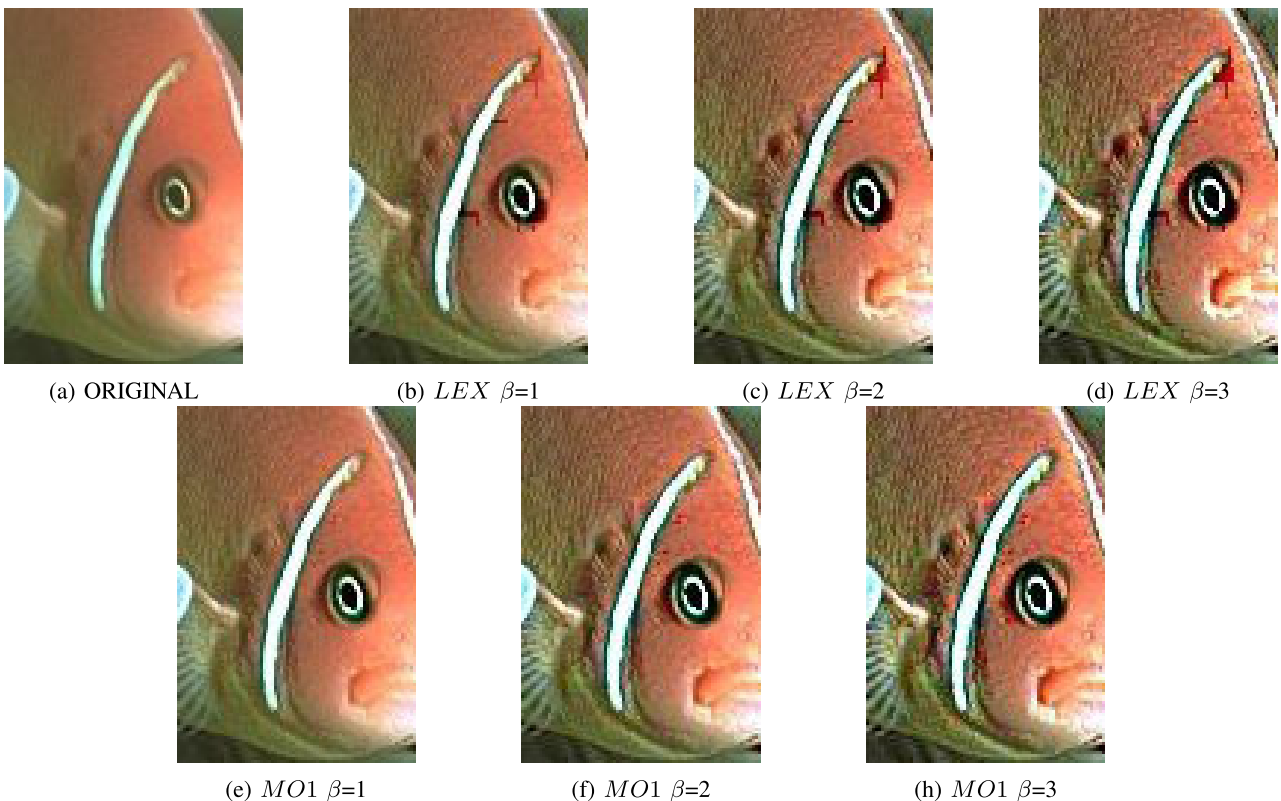


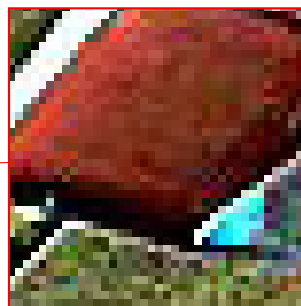
FIGURE 17. Results of applying contrast enhancement. Structuring element 7×7 and domain W_0 .



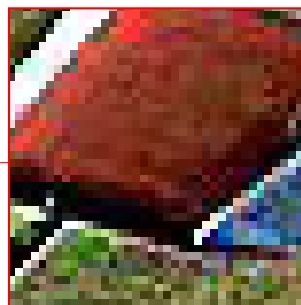
(a) Original image



(b) *ALEX* $\beta=3$



(c) *MO1* $\beta=3$



(d) *MO2* $\beta=3$

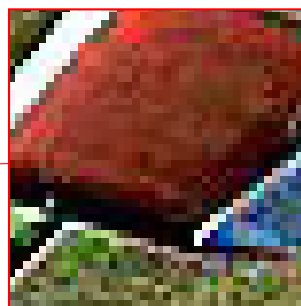


FIGURE 18. Comparison of the ordering method α -lexicographical (*ALEX*) with methods *MO1* and *MO2*.

factor to enhance the image. The larger the structuring element is, the better the obtained results are. In this application, defining the domain as the structuring element (W_0) produces the best results. For this reason only these results are shown in this work. Table 1 lists the average results with the best con-

figurations for the proposed method (*B7WO*), using different weights, along with those of the ordering methods proposed in the literature (*B7*). It presents the 3 best ordering methods proposed in the literature and the 3 best ordering methods obtained by the framework.



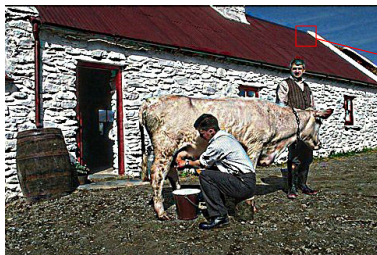
(a) Original image



(b) *ALEX* $\beta=3$



(c) *MO1* $\beta=3$



(d) *MO2* $\beta=3$



FIGURE 19. Comparison of the ordering method α -lexicographical (*ALEX*) with methods *MO1* and *MO2*.

The contrast enhancement method is defined by equation 21 with β equal to 1, 2, 3, 4, 5, 6, and 7. We can see that as β increases, so does the contrast for each of the ordering methods. With β equal to 1, 2, and 3, method *LEX* is more

efficient. However, method *MOD1* is the most efficient, with β equal to 4, 5, 6, and 7.

Figure 17(b-h) also depicts the results when $\beta = \{1, 2, 3\}$ using methods *LEX* and *MO1* (with these values of β the

TABLE 1. Better CIR results.

Ordering	$\beta=1$	$\beta=2$	$\beta=3$	$\beta=4$	$\beta=5$	$\beta=6$	$\beta=7$
LEX	6,528	17,213	26,978	35,207	42,011	47,608	52,217
ALEX	6,527	17,212	26,977	35,206	42,010	47,607	52,216
DLAB	6,516	17,193	26,936	35,150	41,929	47,490	52,070
MOD1	6,445	17,124	26,935	35,213	42,071	47,721	52,361
MOD2	6,441	17,112	26,917	35,194	42,051	47,700	52,344
SMO	6,438	17,069	26,838	35,095	41,931	47,563	52,196

LEX method obtains better results according to the metric *CIR*). LEX method gives more importance to the red component in the ordering; therefore, greater distortions appear in the resulting image (a darker red color in certain areas of the fish face). This kind of distortion is also observed for methods that are lexicographical variations in the *RGB* color space. It should be noted that the level of distortion is lower and details are improved using our proposed method. In Figure 18 and 19 it can be observed the comparison of the ALEX method (the second with the best performance of the literature ordering methods) with the MOD1 and MOD2 methods. It can be observed that the ALEX method adds a false color (turquoise color) on the edges of the wings of the airplane and the roof of the house. The MOD1 and MOD2 methods improve the contrast of the image without adding much distortion.

C. ANALYSIS OF RESULTS

The framework has more flexibility, compared to state of the art methods, for color ordering. This flexibility is due to the different strategies of domain partition, and the information to extract in that domain (generating different ordering options). When comparing the different ordering strategies in the framework, it can be observed that the information and the domain with better performance varies both for Gaussian noise and for speckle noise. In the experiments, it can be observed that almost independently of the type of information extracted from the histograms of each color component, the results of the proposal in the application of noise reduction are better than the comparative state of the art ordering methods, mainly when there is a greater presence of noise.

In the application of contrast enhancement also better results are achieved in terms of contrast enhancement, producing less distortion in the processed image.

V. CONCLUSION AND FUTURE WORK

This paper presented a new *RGB* color image ordering framework. The main strength of this proposal is that the ordering is performed by extracting information from each color component histogram in a certain image domain. In particular, mode, mean, minimum, maximum, variance and smoothness are used to establish a color ordering.

Some tests were performed for two image processing applications: noise reduction and contrast enhancement. Two domain partition strategies were proposed to extract statistical parameters of each color component. The median filter was used for noise elimination and the MAE criterion as numeric evaluation. We establish a robust evaluation for noise

reduction. This evaluation analyzes the performance of the methods when increasing the noise for different noise types. Our method outperformed classical ordering methods encountered in the literature with a considerable amount of Gaussian noise, and for speckle noise we outperform with different statistical parameters from the histograms. The experiments showed that domain partition strategies was not as important as the statistical parameters from the histograms of the color components for obtaining good results.

For the application of contrast enhancement using mathematical morphology, we extend a simple contrast enhancement method proposal by Stojic *et al.* [46], to analyze the enhancement on the image for different contrast values. The extension adds an enhancement factor β , which increases the amount of contrast in the image. The M01 and M02 ordering methods (where the mode is considered) defined here, outperformed the best classical ordering method LEX and its variants according to the *CIR* metric, as the contrast factor β increased. It is worth noting that the framework achieves much less noise than the method LEX and its variants. For this application the best results were obtained from the first domain partition strategy. This strategy consists of extracting information from the order filter window.

Authors are very enthusiastic about the results obtained when using the proposed ordering framework in both noise reduction and contrast enhancement. The results show that the proposed approach is competitive, has in general a better performance and is robust in terms of introducing less distortion in the image. Future works include the extension of the proposed framework to other morphological operations (such as multiscale mathematical morphology) using statistical parameters such as color component histogram entropy, as well as, other applications such as texture classification.

REFERENCES

- [1] M. Livingstone and D. Hubel, "Segregation of form, color, movement, and depth: Anatomy, physiology, and perception," *Science*, vol. 240, no. 4853, pp. 740–749, 1988.
- [2] A. Hanbury and J. Serra, "Mathematical Morphology in the $L^*a^*b^*$ Colour Space," Centre de Morphologie Mathématique Ecole des Mines de Paris, Paris, France, Tech. Rep. N-36/01/MM, 2001.
- [3] A. Hanbury and J. Serra, "Mathematical morphology in the *HLS* colour space," in *Proc. BMVC*, 2001, pp. 1–10.
- [4] A. Hanbury and J. Serra, "Mathematical morphology in the *CIELAB* space," *Image Anal. Stereol.*, vol. 21, no. 3, pp. 201–206, 2002.
- [5] M. C. Tobar, C. Platero, P. M. González, and G. Asensio, "Mathematical morphology in the *HSI* colour space," in *Pattern Recognition and Image Analysis*. Berlin, Germany: Springer, 2007, pp. 467–474.
- [6] T. Lei, Y. Wang, Y. Fan, and J. Zhao, "Vector morphological operators in HSV color space," *Sci. China Inf. Sci.*, vol. 56, no. 1, pp. 1–12, 2013.
- [7] E. Zaharescu, M. Zamfir, and C. Vertan, "Color morphology-like operators based on color geometric shape characteristics," in *Proc. Int. Symp. Signals, Signals, Circuits Syst., (SCS)*, vol. 1, Jul. 2003, pp. 145–148.
- [8] C.-J. Z. X.-H. Gao and X.-Y. Hu, "An adaptive lexicographical ordering of color mathematical morphology," *J. Comput.*, vol. 24, no. 3, pp. 51–59, 2013.
- [9] L. Wang and L. Yan, "Edge detection of color image using vector morphological operators," in *Proc. 2nd Int. Conf. Comput. Sci. Netw. Technol.*, Dec. 2012, pp. 2211–2215.
- [10] E. Aptoula and S. Lefèvre, "A comparative study on multivariate mathematical morphology," *Pattern Recognit.*, vol. 40, no. 11, pp. 2914–2929, 2007.

- [11] F. G. O. Zamora, *Procesamiento Morfológico de Imágenes en Color. Aplicación a la Reconstrucción geodésica*. Alicante, Spain: Miguel de Cervantes Virtual Library, 2002.
- [12] J. L. V. Noguera, H. L. Ayala, C. E. Schaerer, and M. Rolón, "Mathematical morphology for counting trypanosoma cruzi amastigotes," in *Proc. 39th Latin Amer. Comput. Conf. (CLEI)*, Oct. 2013, pp. 1–12.
- [13] A. Ledoux, N. Richard, and A.-S. Capelle-Laize, "Limits and comparisons of orderings using colour distances," *Traitement du Signal*, vol. 29, nos. 1–2, pp. 65–82, 2012.
- [14] J. J. van de Gronde and J. B. T. M. Roerdink, "Group-invariant frames for colour morphology," in *Mathematical Morphology and Its Applications to Signal and Image Processing*. Berlin, Germany: Springer, 2013, pp. 267–278.
- [15] S. Velasco-Forero and J. Angulo, "Random projection depth for multivariate mathematical morphology," *IEEE J. Sel. Topics Signal Process.*, vol. 6, no. 7, pp. 753–763, Nov. 2012.
- [16] S. Velasco-Forero and J. Angulo, "Morphological processing of hyperspectral images using kriging-based supervised ordering," in *Proc. 17th IEEE Int. Conf. Image Process. (ICIP)*, Sep. 2010, pp. 1409–1412.
- [17] B. Burgeth and A. Kleefeld, "Morphology for color images via Loewner order for matrix fields," in *Mathematical Morphology and Its Applications to Signal and Image Processing*. Berlin, Germany: Springer, 2013, pp. 243–254.
- [18] S. Velasco-Forero and J. Angulo, "Supervised ordering in \mathbb{R}^p : Application to morphological processing of hyperspectral images," *IEEE Trans. Image Process.*, vol. 20, no. 11, pp. 3301–3308, Nov. 2011.
- [19] A. G. Hanbury and J. Serra, "Morphological operators on the unit circle," *IEEE Trans. Image Process.*, vol. 10, no. 12, pp. 1842–1850, Dec. 2001.
- [20] J. Angulo, "Pseudo-morphological image diffusion using the counter-harmonic paradigm," in *Advanced Concepts for Intelligent Vision Systems*. Berlin, Germany: Springer, 2010, pp. 426–437.
- [21] E. Aptoula and S. Lefèvre, " α -trimmed lexicographical extrema for pseudo-morphological image analysis," *J. Vis. Commun. Image Represent.*, vol. 19, no. 3, pp. 165–174, Apr. 2008.
- [22] A. Kleefeld and B. Burgeth, "Processing multispectral images via mathematical morphology," in *Visualization and Processing of Higher Order Descriptors for Multi-Valued Data*. Cham, Switzerland: Springer, 2015, pp. 129–148.
- [23] J. L. V. Noguera, H. L. Ayala, C. E. Schaerer, and J. Facon, "A color morphological ordering method based on additive and subtractive spaces," in *Proc. IEEE Int. Conf. Image Process. (ICIP)*, Oct. 2014, pp. 674–678.
- [24] C. Riveros, H. Morel, H. L. Ayala, and J. L. V. Noguera, "Color ordering strategy based on Loewner order applied to the mathematical morphology," in *Proc. 42nd Latin Amer. Comput. Conf. (CLEI)*, Oct. 2016, pp. 1–7.
- [25] E. Aptoula and S. Lefèvre, "On lexicographical ordering in multivariate mathematical morphology," *Pattern Recognit. Lett.*, vol. 29, no. 2, pp. 109–118, Jan. 2008.
- [26] J.-F. Rivest, "Morphological operators on complex signals," *Signal Process.*, vol. 84, no. 1, pp. 133–139, 2004.
- [27] J. Angulo, "Unified morphological color processing framework in a lum/sat/hue representation," in *Mathematical Morphology: 40 Years On*. Dordrecht, The Netherlands: Springer, 2005, pp. 387–396.
- [28] G. Louverdis, M. I. Vardavoulia, I. Andreadis, and P. Tsalides, "A new approach to morphological color image processing," *Pattern Recognit.*, vol. 35, no. 8, pp. 1733–1741, 2002.
- [29] M. I. Vardavoulia, I. Andreadis, and P. Tsalides, "Vector ordering and morphological operations for colour image processing: Fundamentals and applications," *Pattern Anal. Appl.*, vol. 5, no. 3, pp. 271–287, 2002.
- [30] G. Louverdis, I. Andreadis, and P. Tsalides, "Morphological granulometries for color images," in *Proc. 2nd Hellenic Conf. Artif. Intell.*, Apr. 2002, pp. 333–342.
- [31] J. Angulo and J. Serra, "Morphological coding of color images by vector connected filters," in *Proc. 7th Int. Symp. Signal Process. Appl.*, vol. 1, Jul. 2003, pp. 69–72.
- [32] F. Ortiz, F. Torres, and P. Gil, "Gaussian noise elimination in colour images by vector-connected filters," in *Proc. 17th Int. Conf. Pattern Recognit.*, vol. 4, Aug. 2004, pp. 807–810.
- [33] J. Angulo, "Morphological color processing based on distances. Application to color denoising and enhancement by centre and contrast operators," in *Proc. VIIP*, 2005, pp. 314–319.
- [34] L. J. Sartor and A. R. Weeks, "Morphological operations on color images," *J. Electron. Imag.*, vol. 10, no. 2, pp. 548–559, 2001.
- [35] A. Bouchet, P. Alonso, J. I. Pastore, S. Montes, and I. Díaz, "Fuzzy mathematical morphology for color images defined by fuzzy preference relations," *Pattern Recognit.*, vol. 60, pp. 720–733, Dec. 2016.
- [36] P. Bibiloni, M. González-Hidalgo, and S. Massanet, "Soft color morphology: A fuzzy approach for multivariate images," *J. Math. Imag. Vis.*, vol. 61, pp. 394–410, Sep. 2018.
- [37] A. Ledoux and N. Richard, "Color and multiscale texture features from vectorial mathematical morphology," *J. Signal, Image Video Process.*, vol. 10, no. 3, pp. 431–438, 2016.
- [38] H.-C. Shih and E.-R. Liu, "Automatic reference color selection for adaptive mathematical morphology and application in image segmentation," *IEEE Trans. Image Process.*, vol. 25, no. 10, pp. 4665–4676, Oct. 2016.
- [39] A. J. Sanjeevini, S. Saranya, S. Babu, B. Vijayalakshmi, and X. A. Davix, "Automatic reference color selection for adaptive mathematical morphology," *J. Netw. Commun. Emerg. Technol. (JNCET)*, vol. 7, no. 5, pp. 9–13, 2017.
- [40] J. Wang, G. Liang, Y. Wu, Y. Li, and J. Hu, "New colour morphological operators on hypergraph," *IET Image Process.*, vol. 12, no. 5, pp. 690–695, May 2017.
- [41] A. Trémeau, "Analyse d'images couleur: Du pixel à la scène," Univ. Saint-Etienne, Saint-Étienne, France, Tech. Rep., 1998.
- [42] M. L. Comer and E. J. Delp, "Morphological operations for color image processing," *J. Electron. Imag.*, vol. 8, no. 3, pp. 279–289, 1999.
- [43] H. Deborah, N. Richard, and J. Y. Hardeberg, "Spectral ordering assessment using spectral median filters," in *Proc. Int. Symp. Math. Morphol. Appl. Signal Image Process.* Cham, Switzerland: Springer, 2015, pp. 387–397.
- [44] R. K. Sinha, P. Subudhi, and S. Mukhopadhyay, "A morphological color image contrast enhancement technique using Hilbert 3D space filling curve," in *Advanced Computational and Communication Paradigms*. Singapore: Springer, 2018, pp. 453–463.
- [45] J. Chanussot and P. Lambert, "Bit mixing paradigm for multivalued morphological filters," in *Proc. 6th Int. Conf. Image Process. Appl.*, vol. 2, Jul. 1997, pp. 804–808.
- [46] T. Stojic, I. Reljin, and B. Reljin, "Local contrast enhancement in digital mammography by using mathematical morphology," in *Proc. Int. Symp. Signals, Circuits Syst. (ISSCS)*, vol. 2, Jul. 2005, pp. 609–612.
- [47] J. Serra, "Introduction to mathematical morphology," *Comput. Vis., Graph., Image Process.*, vol. 35, no. 3, pp. 283–305, 1986.
- [48] E. Aptoula and S. Lefevre, "Pseudo multivariate morphological operators based on α -trimmed lexicographical extrema," in *Proc. 5th Int. Symp. Image Signal Process. Anal.*, Sep. 2007, pp. 367–372.
- [49] F. G. O. Zamora, F. Torres-Medina, J. Lopez-Angulo, and S. P. Mendez, "Comparative study of vectorial morphological operations in different color spaces," *Intell. Syst. Adv. Manuf.*, vol. 4572, pp. 259–268, Oct. 2001.
- [50] V. Tuzlukov, *Signal Processing Noise*, vol. 8. Boca Raton, FL, USA: CRC Press, 2002.
- [51] W. B. Davenport and W. L. Root, *An Introduction to the Theory of Random Signals and Noise*. New York, NY, USA: McGraw-Hill, 1958.
- [52] J. C. M. Román, H. L. Ayala, and J. L. V. Noguera, "Top-hat transform for enhancement of aerial thermal images," in *Proc. 30th SIBGRABI Conf. Graph., Patterns Images (SIBGRABI)*, Oct. 2017, pp. 277–284.
- [53] J. C. M. Román, J. L. V. Noguera, H. Legal-Ayala, D. P. Pinto-Roa, S. Gomez-Guerrero, and M. G. Torres, "Entropy and contrast enhancement of infrared thermal images using the multiscale top-hat transform," *Entropy*, vol. 21, no. 3, p. 244, 2019.
- [54] T. Chen, Q. Wu, R. Rahmani-Torkaman, and J. Hughes, "A pseudo top-hat mathematical morphological approach to edge detection in dark regions," *Pattern Recognit.*, vol. 35, no. 1, pp. 199–210, 2002.
- [55] C. J. Willmott and K. Matsuura, "Advantages of the mean absolute error (MAE) over the root mean square error (RMSE) in assessing average model performance," *Climate Res.*, vol. 30, no. 1, pp. 79–82, Dec. 2005.
- [56] P. Arbelaez, C. Fowlkes, and D. Martin. (2007). *The Berkeley Segmentation Dataset and Benchmark*. [Online]. Available: <http://www.eecs.berkeley.edu/Research/Projects/CS/vision/bsds>
- [57] Y.-P. Wang, Q. Wu, K. R. Castleman, and Z. Xiong, "Chromosome image enhancement using multiscale differential operators," *IEEE Trans. Med. Imag.*, vol. 22, no. 5, pp. 685–693, May 2003.



JOSÉ LUIS VÁZQUEZ NOGUERA was born in Asunción, Paraguay, in 1985. He received the degree in computer systems engineering from the Instituto Tecnológico de León, México, in 2008, and the M.Sc. and Ph.D. degrees in computer science from the Universidad Nacional de Asunción, Paraguay, in 2012 and 2018, respectively. He has authored over 20 articles in image processing, mathematical morphology, and computer vision.



CHRISTIAN E. SCHAEERER was born in Asunción, Paraguay, in 1970. He received the degree in electromechanical engineering from the National University of Asunción (UNA), Paraguay, in 1996, and the M.Sc. and D.Sc. degrees in electrical engineering from the Federal University of Rio de Janeiro, Brazil, in 1998 and 2002, respectively. He held a postdoctoral position, in 2003, and was an Associate Researcher, from 2004 to 2007, in applied mathematics with the Instituto de

Matemática Pura e Aplicada (IMPA), Rio de Janeiro, Brazil. Since 2008, he has been a Research Professor with UNA. He is currently a Team Leader and the Founder of the Scientific and Applied Computing Laboratory and the Núcleo de Investigación Científica y Tecnológica (NIDTEC), Polytechnic School, UNA. He has authored over 40 articles in simulation and control, parallel computing, and control theory. He is the President of the Paraguayan Mathematical Society and the Vice President of the PanAmerican Association for Computational Interdisciplinary Sciences. He is a member of several scientific commissions and received several awards, and recently, he was awarded for his contribution to the scientific-industry enforcement.



JACQUES FACON was born in Mazingarbe, France, in 1961. He received the degree in computer engineering from the Ecole Supérieure d'Ingénieurs em Génie Électrique de Rouen (ESIGELEC), France, in 1984, the M.Sc. degree in electrical engineering from the Université de Rouen, France, in 1984, and the Ph.D. degree in electrical engineering from the Université de Technologie de Compiègne (UTC), França, in 1987. Since 2018, he has been a Research Professor with

the Departamento de Computação e Eletrônica, Universidade Federal do Espírito Santo (UFES), Brazil. He has authored over 40 articles in image processing, mathematical morphology, and computer vision.



HORACIO LEGAL AYALA (M'12) was born in Asunción, Paraguay, in 1965. He received the degree in electrical engineering from the Federal University of Parana, Brazil, in 1989, the M.Sc. degree in electrical engineering and industrial informatics from the Federal Technological University of Parana, Curitiba, Brazil, in 1991, and the Ph.D. degree in applied informatics from the Pontifical Catholic University of Parana, Curitiba, in 2004. Since 2007, he has been an Associate Professor and an Academic Coordinator of the Graduate Program in Computer Science at the Polytechnic School, National University of Asunción, Asunción. He has authored over 40 articles in image processing, mathematical morphology, and computer vision.

...